Comparison of Surface Models and Skeletal Models for Inertial Sensor Data Synthesis

Lena Uhlenberg
FAU Erlangen-Nürnberg
Germany
lena.uhlenberg@web.de

Oliver Amft
University of Freiburg, Germany
Hahn-Schickard, Germany
amft@ieee.org

***Abstract*—We present a modelling and simulation framework to synthesise body-worn inertial sensor data based on personalised human body surface and biomechanical models. Anthropometric data and reference images were used to create personalised body surface mesh models. The mesh armature was aligned using motion capture reference pose and afterwards mesh and armature were parented. In addition, skeletal models were created using an established musculoskeletal dynamic modelling framework. Four activities of daily living (ADL), including upper and lower limbs were simulated with surface and skeletal models using motion capture data as stimuli. Acceleration and angular velocity data were simulated for 12 body areas of surface models and 8 body areas of skeletal models. We compared simulated inertial sensor data of both models against physical IMU measurements that were obtained simultaneously with video motion capture. Results showed average errors of $27\,^{\circ}/s$ vs. $31\,^{\circ}/s$ and $1.7\,m/s^2$ vs. $3.3\,m/s^2$ for surface and skeletal models, respectively. Mean correlation coefficients of body surface models ranged between 0.2 – 0.9 for simulated angular velocity and between 0.1 – 0.8 for simulated acceleration when compared to physical IMU data. The proposed surface modelling consistently showed similar or lower error compared to established skeletal modelling across ADLs and study participants. Body surface models can offer a more realistic representation compared to skeletal models for simulation-based analysis and optimisation of wearable inertial sensor systems.**

***Index Terms*—Accelerometer, gyroscope, multiscale modelling**

I. Introduction

Biomechanical models can provide a basis for evaluating wearable system design, e.g. to analyse the performance of digital biomarker estimation algorithms depending on the wearable sensor position [1]. Validated musculoskeletal models are provided, e.g. by the open-source OpenSim platform (https://simtk.org/projects/opensim) [2]. However, the biomechanical models provide a skeletal representation only, thus do not account for individual body surfaces. Another branch of modelling approaches emerged from 3D/4D computer graphics with the intend to create realistic animations and visual effects, e.g. by scanning human bodies. The latter models lack a validated biomechanical basis. For example, Blender's open-source software tools (http://www.blender.org) were used to create animated films, among others. Recently Blender was used to rig statistical shape models and control surface models by an inverse kinematic solver [3].

In this work, we combine biomechanical modelling based on video motion capture (MoCap) marker data and surface modelling towards improved validity of inertial sensor synthesis. In particular, this paper provides the following contributions:

1) We present a modelling and simulation framework to synthesise inertial sensor data based on personalised body surface models, created from biomechanical and anthropometric data. We simulate sensor data of inertial measurement units (IMUs), including triaxial acceleration sensors and triaxial transducers of angular velocity.
2) We analyse sensor synthesis performance by comparing generated inertial sensor data from the surface model against simultaneous inertial and MoCap measurements from five study participants in different activities of daily living (ADLs). In addition, we compare synthesis performances of surface models and skeletal models. Personalised surface models and skeletal models were created for each study participant.

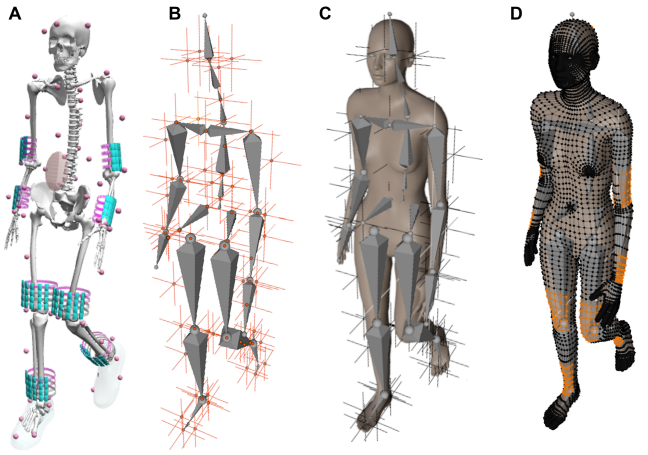

Fig. 1. Overview of modelling approaches. A: Skeletal model with simulated IMU cubes. B: Armature of surface model posed by MoCap Empties. C: Surface model with rigged armature. D: Frontal view faces of body areas of interest used to synthesise inertial sensors.

II. Related work

Different approaches have been investigated for sensor synthesis, focusing on optimal sensor positioning and data augmentation for machine learning. Mundt et al. [4] estimated joint kinematics and kinetics using musculoskeletal models to simulate acceleration and angular velocity data from five selected sensor positions as input for an artificial neural

network. Their results showed that the simulation approach is a valid method for data augmentation in biomechanics. Hoareau et al. [5] compared simulated IMU data with real IMU data for motion classification based on statistical features extracted from the time series signal. Sharifi Renani et al. [6] compared synthetic and measured IMU data during walking to increase accuracy in deep learning models for joint kinematic predictions. OpenSim was used to generate synthetic IMU data with known relative orientation and displacement of the inertial sensors tracked by markers. Zimmermann et al. [7] proposed an IMU-to-segment mapping and orientation alignment for the lower body. Kwon et al. [8] presented IMUTube, an automated processing pipeline to convert video of human activity into virtual streams of IMU data. Lämsä et al. [9] used neural networks to generate IMU signals and features from monocular videos of human activities. However, there are persisting challenges concerning validity and variability of data augmentation for sensor time series [10] and simulated data is often used for augmentation during model training only.

In this work, we consider personalised inverse kinematic models to synthesise inertial sensors at all limbs. Compared to previous work, our simulation approach includes personalised surface models based on anthropometric data that are animated based on the inverse kinematic models. Moreover, we analyse several ADLs besides walking, which has been primarily considered so far. The selected ADLs include complex movement sequences that occur in everyday life, and thus provide insight into IMU capture of participant mobility.

III. Methods

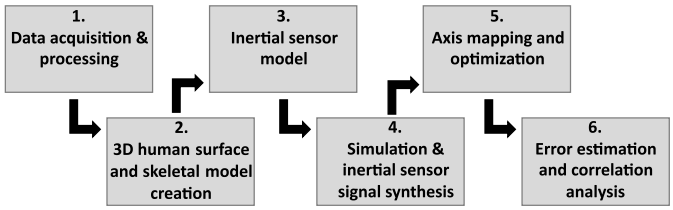

Fig. 2. Framework overview. MoCap data were obtained and processed to create 3D human surface models and skeletal models. Body areas of interest were defined to connect inertial sensor model instances to surface models. Motion marker data was used to simulate ADLs and synthesise inertial sensors. Simulated inertial data was mapped to physical IMU measurements and residual error as well as correlation were analysed.

Our surface modelling framework consists of six steps (Fig. 2). Initially, MoCap data was collected, processed and joint centres were calculated using standard biomechanical equations. Subsequently, anthropometric data and MoCap data was used to create a 3D body surface model and a skeletal model. Inertial sensor model instances were created, comprising positions and orientations of simulated sensors within body areas of interest. To find a simulated sensor that best matches a physical IMU, axis mapping was applied across all synthesised sensors within a body area of interest, i.e. a search region around each physical IMU. Finally, synthesis performance was estimated by deriving residual error and correlation based on the simulated and measured sensor timeseries per ADL.

A. Surface model

Anthropometric data and reference images were used to create the body surface mesh model in the open-source software MakeHuman (http://www.makehumancommunity.org). Every created mesh model contained one mesh and one rigged armature. Mesh vertices of the created surface models correspond to constant anatomical positions on the body surface. Mesh models were subsequently imported into Blender and unparented so that the armature could be separately aligned using Empties from MoCap markers static trial (reference pose). The original mesh import was replaced by a second import of the mesh model as reference poses of MakeHuman and the MoCap data were not identical (Fig. 3C). The newly imported mesh was manually fitted to the reference pose and body circumferences indicated by Empties of the static trial (Fig. 3D). Once an optimal alignment of mesh and Empties was achieved the mesh and the armature of the original import were parented with automatic weight distribution across vertices. The resulting model pose was set as new reference pose.

B. Skeletal model

For skeletal models, an existing OpenSim full-body thoracolumbar spine model, as described by Schmid et al. [12], was used. The model was selected to account for the degrees of freedom at upper extremities and spine area. Since the original body model represents bones, joints, and muscle links only, an auxiliary structure with a cylindrical shape was designed to approximate limb surfaces. At the auxiliary structure, 4 rings with 5-6 positions per ring were defined to attach sensors represented by cubes (Fig. 1A).

C. Inertial sensor model

A global 3D Cartesian coordinate frame G with coordinate axes (x,y,z) was defined, besides a body-local frame L, to support spatial representation of the surface model and the skeletal model, respectively.

An additive signal model was used to represent acceleration signals, where $\vec{a}(t) = (a_x, a_y, a_z)$ is the sum of the sensor's dynamic acceleration $\vec{a}_d(t)$ and the equivalent gravitational component $\vec{a}_g(t)$ acting on the sensor device, according to $\vec{a}(t) = \vec{a}_d(t) + \vec{a}_g(t)$. Vector $\vec{k}(t) = (k_x(t), k_y(t), k_z(t))$ is a position vector at time t of a simulated sensor instance, i.e face normal for surface models and main surface normal for skeletal model cubes. Dynamic acceleration $\vec{a_d}(t)$ was synthesised from the second derivative of vector $\vec{k(t)}$ following $\vec{a_d}(t) = \frac{d^2\vec{k}(t)}{dt^2}$. The static acceleration component $\vec{a}_g(\mathrm{t})$ was computed by mapping sensor orientation taken from rotation matrix ($Q_L^G \in \mathbb{R}^{3x3}$) to the gravity-carrying axis ($\vec{j} = (0, 1, 0)$), i.e. along the y-axis of the global coordinate frame G. Rotation matrix Q_L^G was derived via quaternion rotation from face normal and cube normal position vectors, respectively. The resulting unit vector $\vec{k}_j \in \mathbb{R}^{3x3}$ represents a per-axis gravity contribution:

$$\vec{k_j}(\mathrm{t}) = Q_L^G \vec{k}(t) \cdot \vec{j}. \quad (1)$$

Unit vector $\vec{k}_j(t)$ was used to obtain $\vec{a_g}(t)$ for all sensor axes with $g = 9.81\,m/s^2$ according to $\vec{a}_g(t) = \vec{k_j}(t) \cdot g$. Angular velocity, as measured by gyroscope sensors, was synthesised by deriving orientation estimates with respect to time:

$$\vec{\omega}(t) = \frac{dQ_L^G \vec{k}(t)}{dt}, \quad (2)$$

where $Q_L^G \vec{k}(t)$ refers to the simulated sensor orientation and satisfies $(Q_L^G)^{-1} = (Q_L^G)^T$ as well as $\det(Q_L^G) = 1$ [11].

For surface models, we derived sensor positions by selecting face normals within body areas of interest (see Figs. 1D and 3E). For skeletal models, sensors were designed as inertia-free $5\,mm^3$ cubes and scaled in volume by factors of 0.001, 0.005, and 0.003 in x-, y-, and z-axis, respectively. Sensor cubes were uniformly positioned at models using parameterised coordinates according to the auxiliary limb structure. We virtually attached 24 sensors at each upper and lower leg and 20 sensors at each upper and lower arm by direct-link (WeldJoint), resulting in a total of 88 simulated sensors, see Fig. 1A.

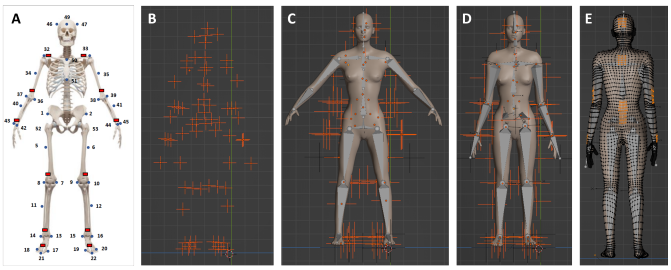

Fig. 3. A: Marker setup used for MoCap and body model construction. B: Imported MoCap marker Empties in Blender (without IMU instances). C: Mesh and rigged armature of MakeHuman reference pose with Empties of static MoCap trial. D: Mesh and rigged armature after manual adjustment matched to static MoCap trial. E: Highlighted faces indicate body areas of interest in rear view (see also Fig. 1D).

D. Simulation and inertial sensor synthesis

Simulations of surface and skeletal models were performed using MoCap marker data of study participants, while performing different ADLs. To track marker movement during surface modelling, bone constraints were added to the armature. Acceleration and angular velocity data were synthesised at 100 Hz.

E. Axis mapping

Within each body area of interest the best matching surface position and cube position were found by minimising the root mean squared error (RMSE) of simulated sensor data against the respective physical IMU sensor data. A search was performed for each participant and ADL, across all sensor axis permutations, e.g., (x,y,z), (y,z,x), and including all axis inversions, e.g., (-x,y,z), (x,-y,z). For angular velocity in both models and acceleration in skeletal models, 48 axis combinations were searched (6 axis permutations and 8 axis inversions). For acceleration in surface models, 2304 axis combinations (6x6 axis permutations times 8x8 axis inversions) were searched as gravity axis $\vec{k_j}$ and thus static acceleration could vary per sensor position.

Between $59-119$ face normals were extracted for each body area of interest that ranged in area between $29.5\,cm^2$ at forearms and $146.2\,cm^2$ at thighs. Corresponding surface model face area ranged between $0.85\,cm^2$ and $6.1\,cm^2$. Figure 3E and Fig. 1D illustrate all body areas of interest. Based on [1] for skeletal models, sensor cube positions on arms and legs were adjusted to body areas of interest around approximate physical IMU positions (see Fig. 1A).

F. Data set

Five healthy study participants were considered in this work. All participants gave written consent prior to participation and ethics approval was granted by the institutional ethics committee. Anthropometric data of the participants were collected to derive body segment masses and joint centres using Visual3D (C-Motion Inc., Germantown, MD, USA). Table I details participant data.

TABLE I
ANTHROPOMETRIC DATA OF PARTICIPANTS. F: FEMALE. M: MALE. BMI: BODY MASS INDEX.

ID	Height [m]	Weight [kg]	Age [years]	Sex [F/M]	BMI [kg/m^2]	Leg length right [m]	Leg length left [m]
P1	1.72	56	29	F	18.93	0.90	0.90
P2	1.71	56	23	F	19.15	0.95	0.94
P3	1.72	67	27	M	22.65	0.89	0.88
P4	1.72	86	25	M	29.07	1.00	1.00
P5	1.65	62	28	F	22.77	0.90	0.89
Means	**1.70**	**65.40**	**26.40**	**(F=3; M=2)**	**22.51**	**0.93**	**0.92**

G. Data acquisition and processing

In total 54 reflective spherical markers were placed at anatomical landmarks according to the marker setup shown in Fig. 3A. A synchronized and calibrated 11-camera marker-based MoCap system (ten Oqus7+ infrared cameras and one Oqus5+ highspeed camera, Qualisys AB, Gothenburg, Sweden) was used to acquire gold-standard MoCap data at a frame rate of 100 Hz. The MoCap system was time-synchronized with 16 IMUs (MyoMotion, Noraxon, AZ, USA), attached at each body segment to measure acceleration and angular velocity.

Prior to each measurement, a static reference trial was performed to reconstruct segments and define dimensions, joint centers, and segment coordinate system, as well as to calibrate IMU sensors. Subsequently, participants were asked to perform four different ADLs involving upper and lower limb movements: shelve ordering (SO), stairs ascending (SA), stairs descending (SD), and walking (W).

Data pre-processing, including labelling and gap filling was conducted using Qualysis Track Manager, v. 2018. Subsequently, a 6-degree of freedom inverse kinematics constrained model (IOR Multi-Segment Trunk [13] and a Conventional Gait Model with CODA pelvis model [14] were created using Visual3D (Fig. 3C). The models served as input data (i.e to calculate joint centers) for surface modelling. MoCap data was filtered (6 Hz lowpass Butterworth filter), converted and

imported as Empties into Blender (Fig. 3D). Maker MoCap data was imported into OpenSim to create skeletal models.

H. Error estimation and correlation analysis

Synthesis performance was evaluated for both surface and skeletal models by deriving RMSE between simulated sensor timeseries after axis mapping and physically measured inertial sensor timeseries for each sensor type, body area of interest, participant, and ADL. Furthermore, Pearson correlation coefficients were calculated. RMSE and correlation analyses were averaged across sensor axes.

IV. Results

Figure 4 shows an excerpt of simulated angular velocity timeseries from surface ($\vec{\hat{\omega}}_{\mathrm{SU}}(t)$) and skeletal ($\vec{\hat{\omega}}_{\mathrm{SK}}(t)$) models, compared to measured IMU sensor timeseries ($\vec{\omega}(t)$). Overall, measured and simulated timeseries patterns were in agreement across all sensor positions for both surface and skeletal models. Certain deviations, in particular during dynamic movements, are however observable. Figure 5 shows an excerpt of simulated acceleration signals for surface ($\vec{\hat{a}}_{\mathrm{SU}}(t)$) and skeletal ($\vec{\hat{a}}_{\mathrm{SK}}(t)$) models, compared to measured IMU sensor timeseries ($\vec{a}(t)$). Here too, timeseries are in agreement, with larger visible deviations for $\vec{\hat{a}}_{\mathrm{SK}}(t)$ compared to $\vec{\hat{a}}_{\mathrm{SU}}(t)$.

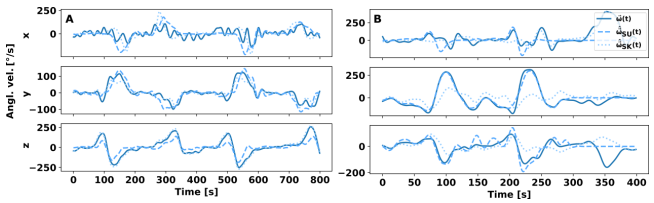

Fig. 4. Excerpt of measured ($\vec{\omega}(t)$) and simulated timeseries for surface ($\vec{\hat{\omega}}_{\mathrm{SU}}(t)$) and skeletal ($\vec{\hat{\omega}}_{\mathrm{SK}}(t)$) models. A: Upper arm position during shelve ordering of Participant P1. B: Shank position during stairs ascending of Participant P4.

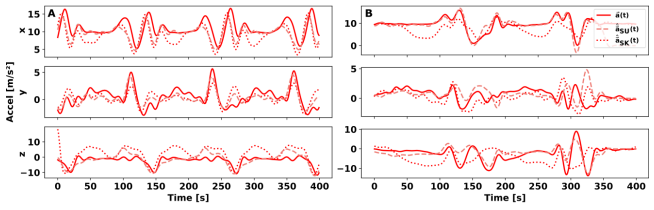

Fig. 5. Excerpt of measured ($\vec{a}(t)$) and simulated timeseries for surface ($\vec{\hat{a}}_{\mathrm{SU}}(t)$) and skeletal ($\vec{\hat{a}}_{\mathrm{SK}}(t)$) models. A: Shank position during stairs ascending of Participant P2. B: Thigh position during walking of Participant P3.

Table II summarises RMSE and correlation results of surface and skeletal models per ADL at limbs. Surface models showed overall lower RMSE compared to skeletal models for angular velocity ($> 4.3°/s$) and acceleration ($> 1.5\,m/s^2$). Surface models were superior for stairs ascending (SA) and stairs descending (SD). For shelve ordering (SO) agreement for angular velocity from skeletal models was larger than for surface models. For SO acceleration, both models performed similarly. For walking (W), both models showed similar

TABLE II

RMSE mean and sd as well as minimum and maximum Pearson correlation coefficients r of simulated sensor timeseries for surface and skeletal models at limbs across all participants.

Model	ADL	Angl. vel ($°/s$)				Acc (m/s^2)			
		RMSE		r		RMSE		r	
		Mean	SD	Min	Max	Mean	SD	Min	Max
Surface model (SU)	SO	23.93	0.2	0.10	0.70	1.57	0.18	0.07	0.74
	SA	24.93	0.17	0.20	0.91	1.35	0.09	0.31	0.80
	SD	24.29	0.16	0.18	0.88	1.94	0.15	0.44	0.83
	W	33.77	0.11	0.29	0.91	2.08	0.14	0.35	0.74
	Mean	**26.73**	**0.16**	**0.19**	**0.85**	**1.74**	**0.14**	**0.29**	**0.78**
Skeletal model (SK)	SO	18.64	0.26	0.30	0.78	1.8	0.16	0.12	0.68
	SA	33.84	0.1	0.20	0.95	3.18	0.11	0.15	0.68
	SD	36.38	0.11	0.16	0.92	3.98	0.12	0.22	0.74
	W	35.37	0.14	0.49	0.91	4.35	0.17	0.24	0.72
	Mean	**31.06**	**0.15**	**0.29**	**0.89**	**3.33**	**0.14**	**0.19**	**0.70**

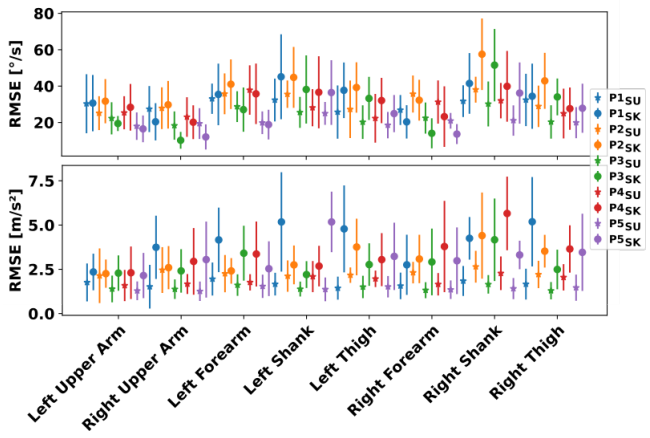

Fig. 6. Comparison of simulated sensor data RMSE of surface (SU) and skeletal (SK) models per participant (P1-P5), body position, and sensor type, averaged over all ADLs. A: Angular velocity RMSE mean and sd. B: Acceleration RMSE mean and sd.

angular velocity errors, while surface models yielded lower acceleration error.

Figure 6 compares sensor synthesis performance of surface and skeletal models per participant and body position, averaged over all ADLs. For most participants and body positions surface models yielded lower error than skeletal models. Variability between participants was observed but no clear relation to anthropometric variables could be made.

Figure 7 shows sensor synthesis performance averaged across all five participants and all sensor positions of surface models. The analysis includes additional body positions included in the surface modelling (cf. Fig. 3). Angular velocity and acceleration of shelve ordering (SO) yielded the lowest RMSE for all sensor positions, except upper arms and forearms, which can be explained by the specific movement. Overall, the more body segments are involved in an ADL, the larger the RMSE mean and sd. Mean RMSE across all sensor positions ranged between $17.98\,°/s$ – $26.8\,°/s$ and $1.42\,m/s^2$ – $1.9\,m/s^2$.

V. Discussion and Conclusions

We introduced a sensor synthesis framework based on human body surface models and demonstrated its utility in different ADLs. Surface representations were generated based

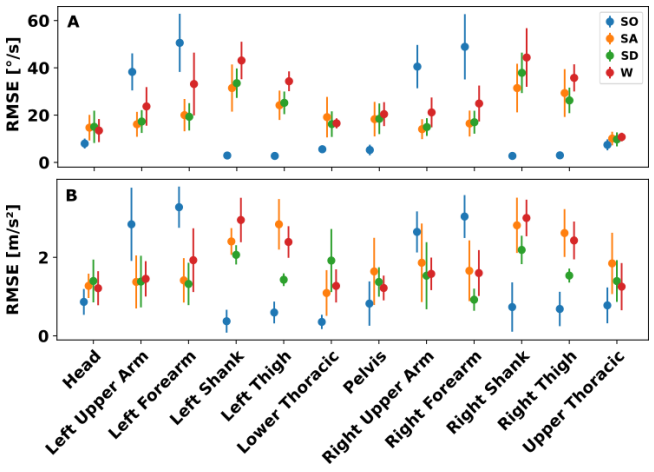

Fig. 7. A: Angular velocity RMSE mean and sd for all ADLs per sensor position averaged over patients for surface models. B: Acceleration RMSE mean and SD for all ADLs per sensor position averaged over patients for surface models. SO: Shelve ordering. SA: Stairs ascending. SD: Stairs descending. W: walking.

on anthropometric data, i.e. without 3D body scanning. Kinematic behaviour of our surface models was derived from validated biomechanical modelling. We compared simulated inertial sensor data of the surface models against physical IMU measurements and established skeletal models. Results showed average errors of $26.7\,°/s$ vs. $31.1\,°/s$ for angular velocity and $1.7\,m/s^2$ vs. $3.3\,m/s^2$ for acceleration for surface and skeletal models, respectively (Tab. II). Overall, the proposed surface modelling approach outperformed existing skeletal models. Only for shelf ordering, surface models showed a larger error compared to skeletal models, however errors remained in a similar band, highlighting that surface models are feasible for synthesising inertial sensors.

RMSE and correlations observed in our analysis are within ranges reported in literature, although previous work primarily analysed walking only. Sharifi Renani et al. [6] compared synthetic and measured IMU data at the pelvis, thigh, shank, and foot during walking. RMSE for angular velocity ranged between $22.9°/s$ – $58.4°/s$ depending on sensor positioning. Correlations ranged between 0.29 – 0.98. RMSE for acceleration ranged between $0.62\,m/s^2$ – $2.46\,m/s^2$ with correlations between 0.75 – 0.96. Zimmermann et al. [7] reported Pearson correlations also during walking, averaged across all IMUs (feet, shanks, thighs, and pelvis) at 0.57 for accelerometers and 0.93 for gyroscopes. Average RMSE across all IMUs was $4.02\,m/s^2$ and $35°/s$ for acceleration and angular velocity. Authors attributed the synthetic gap to additional artifacts due to clothing and soft-tissue that cause additional accelerations.

Our results showed inter-individual simulation error variability (Fig. 6), which could be partly attributed to varying BMI, as P1 had the lowest and P4 the highest BMI. However, error variability may be caused as well by individual body proportion variations that were not accurately captured. Based on the promising performance results for surface models shown in our present work, further investigations could address body parts that are profoundly affected by soft tissue variations, including abdomen, breast, and upper thighs. Moreover, surface modelling could be used in the future to improve garment fitting evaluation under motion dynamics or to investigate body-sensor attachment. By using open-source Blender toolboxes and frameworks, our approach enhances reproducibility compared to previously published modelling and simulation techniques, in particular with regard to a more complex ADL movement analysis.

Acknowledgment

We thank Nina Goes, Juan Carlos Suarez Mora, as well as FAU LTD group and Med 3 of the University Medical Center Erlangen for their support in the study implementation and data preprocessing.

References

[1] A. Derungs and O. Amft, "Estimating wearable motion sensor performance from personal biomechanical models and sensor data synthesis," Nat. Sci. Rep., vol. 10, no. 11450, 2020, doi: 10.1038/s41598-020-68225-6.

[2] A. Seth et al., "OpenSim: Simulating musculoskeletal dynamics and neuromuscular control to study human and animal movement," PLoS Comput. Biol., vol. 14, no. 7, p. e1006223, 2018, doi: 10.1371/journal.pcbi.1006223.

[3] L. Briceno and G. Paul, "MakeHuman: A Review of the Modelling Framework: Volume V: Human Simulation and Virtual Environments, Work With Computing Systems (WWCS), Process Control," 2019, pp. 224–232.

[4] M. Mundt et al., "Estimation of Gait Mechanics Based on Simulated and Measured IMU Data Using an Artificial Neural Network," Front. Bioeng. Biotechnol., vol. 8, 2020, doi: 10.3389/fbioe.2020.00041.

[5] D. Hoareau, G. Jodin, P.-A. Chantal, S. Bretin, J. Prioux, and F. Razan, "Synthetized inertial measurement units (IMUs) to evaluate the placement of wearable sensors on human body for motion recognition," J. Eng., vol. n/a, no. n/a, 2021, doi: 10.1049/tje2.12137.

[6] M. Sharifi Renani, A. M. Eustace, C. A. Myers, and C. W. Clary, "The Use of Synthetic IMU Signals in the Training of Deep Learning Models Significantly Improves the Accuracy of Joint Kinematic Predictions," Sensors, vol. 21, no. 17, p. 5876, Jan. 2021, doi: 10.3390/s21175876.

[7] T. Zimmermann, B. Taetz, and G. Bleser, "IMU-to-Segment Assignment and Orientation Alignment for the Lower Body Using Deep Learning," Sensors, vol. 18, no. 1, p. 302, Jan. 2018, doi: 10.3390/s18010302.

[8] H. Kwon et al., "IMUTube: Automatic Extraction of Virtual on-body Accelerometry from Video for Human Activity Recognition," arXiv.org, May 2020, Accessed: Aug. 12, 2020.

[9] A. Lämsä, J. Tervonen, J. Liikka, C. Álvarez CaSDdo, and M. Bordallo Lopez, Video2IMU: Realistic IMU features and signals from videos. 2022.

[10] B. K. Iwana and S. Uchida, "An empirical survey of data augmentation for time series classification with neural networks," PLoS ONE, vol. 16, no. 7, Jul. 2021, doi: 10.1371/journal.pone.0254841.

[11] S. Zhao, "Time Derivative of Rotation Matrices: A Tutorial," arXiv.org, Sep. 2016, Accessed: Jan. 28, 2022. [Online]. https://arxiv.org/abs/1609.06088v1

[12] S. Schmid, K. A. Burkhart, B. T. Allaire, D. Grindle, and D. E. Anderson, "Musculoskeletal full-body models including a detailed thoracolumbar spine for children and adolescents aged 6 - 18 years," 3rd Int. Workshop Spine Load. Deform., vol. 102, p. 109305, Mar. 2020, doi: 10.1016/j.jbiomech.2019.07.049.

[13] A. Leardini, F. Biagi, A. Merlo, C. Belvedere, and M. G. Benedetti, "Multi-segment trunk kinematics during locomotion and elementary exercises," Clin. Biomech., vol. 26, no. 6, pp. 562–571, Jul. 2011, doi: 10.1016/j.clinbiomech.2011.01.015.

[14] "Tutorial: Building a Conventional Gait Model - Visual3D Wiki Documentation." https://c-motion.com/v3dwiki/index.php?title=Tutorial:_Building_a_Conventional_Gait_Model#Conventional_Gait_Model_Decisions/.